Biol. Cybern. 92, 21–37 (2005)
DOI 10.1007/s00422-004-0526-y

Biological Cybernetics

A model of the saccade-generating system that accounts for trajectory variations produced by competing visual stimuli

Kuniharu Arai, Edward L. Keller

The Smith-Kettlewell Eye Research Institute, 2318 Fillmore Street, San Francisco, CA 94115, USA

Received: 26 February 2004 / Accepted: 28 September 2004 / Published online: 10 December 2004

Abstract. Variable saccade trajectories are produced in visual search paradigms in which multiple potential target stimuli are present. These variable trajectories provide a rich source of information that may lead to a deeper understanding of the basic control mechanisms of the saccadic system. We have used published behavioral observations and neural recordings in the superior colliculus (SC), gathered in monkeys performing visual search paradigms, to guide the construction of a new distributed model of the saccadic system. The new model can account for many of the variations in saccade trajectory produced by the appearance of multiple visual stimuli in a search paradigm. The model uses distributed feedback about current eye motion from the brainstem to the SC to reduce activity there at physiologically realistic rates during saccades. The long-range lateral inhibitory connections between SC cells used in previous models have been eliminated to match recent physiological evidence. The model features interactions between visually activated multiple populations of cells in the SC and distributed and topologically organized inhibitory input to the SC from the SNr to produce some of the types of variable saccadic trajectories, including slightly curved and averaging saccades, observed in visual search tasks. The distributed perisaccadic disinhibition of SC from the substantia nigra (SNr) is assumed to have broad spatial tuning. In order to produce the strongly curved saccades occasionally recorded in visual search, the existence of a parallel input to the saccadic burst generators in addition to that provided by the distributed input from the SC is required. The spatiotemporal form of this additional parallel input is computed based on the assumption that the input from the model SC is realistic. In accordance with other recent models, it is assumed that the parallel input comes from the cerebellum, but our model predicts that the parallel input is delayed during highly curved saccadic trajectories.

Correspondence to: E. L. Keller
(e-mail: elk@ski.org,
Tel.: +1-415-3452102, Fax: +1-415-3458455)

1 Introduction

Previous distributed models of the saccadic system have used lateral inhibitory connections within the superior colliculus (SC) to insure that only a single locus of activity is present on the collicular motor map by the time of saccade onset (Van Opstal and Van Gisbergen 1989; Arai et al. 1994; Optican 1994; Massone and Khoshaba 1995; Grossberg et al. 1997; Bozis and Moschovakis 1998; Arai et al. 1999; Badler and Keller 2002). This type of behavior on a neural map is called winner-take-all. The question naturally arises as to what happens when such a map is stimulated simultaneously with two equally salient visual stimuli. The result is often an "averaging saccade," which lands somewhere in between the spatial locations of the two visual targets (see Chou et al. 1999 for a summary of results in this area). Collicular maps with local excitation and longer-range lateral inhibition predict that the two loci of activity generated by the visual stimuli will inhibit each other, but both will excite the locus on the map between the two regions of visual activation (Van Opstal and Van Gisbergen 1989; Arai et al. 1994; Das et al. 1996; Bozis and Moschovakis 1998). The result will be that these two loci of SC activity will coalesce into a single active site located between the original two.

Recent neurophysiological evidence from single-neuron recording experiments in the monkey do not support this model-based prediction of a single locus of neural activity on the SC motor map during averaging movements. Instead, the distribution of activity on the SC better approximates the two separate loci of activity induced on the SC by the visual stimuli than a single site of activity in between the location of the visually induced activities, even by the time of saccade onset (Edelman and Keller 1998). Similar results that show activity at multiple sites on the SC during saccades have been found in a search task with multiple visual stimuli (McPeek and Keller 2002a; McPeek et al. 2003) and during the highly curved saccades produced in a double-step paradigm (Port and Wurtz 2003). Furthermore, results obtained from a collicular slice preparation and the focal release by photostimulation of the inhibitory transmitter, GABA, suggest

that strong, long-range inhibitory interconnections within the intermediate layers of the SC may not exist (Özen et al. 2004). Extracellular electrical stimulation studies, in contrast, show the existence of extensive long-range inhibitory connections within the SC (Munoz and Istvan 1998). Özen et al. (2004) argue that these inhibitory responses result from activation of passing inhibitory axons from the substantia nigra pars reticulata (SNr) by the extracellularly generated currents.

Although this issue has not been settled, we believe that an absence of or limited intrinsic, long-range inhibitory connections would contribute to the maintained presence of multiple sites of collicular activity found in the recent studies already cited. For our current model we will assume that such connections do not exist. The new distributed model retains some short-range inhibition. Local excitatory interconnections among SC neurons are also retained. The size of the activated region in the SC during saccades has been shown in neurophysiological studies to occupy a third or more of one colliculus and is relatively invariant in spatial extent as a function of saccade size or direction (Anderson et al. 1998). The surround inhibition that helps shape the size of the region of collicular space activated by single visual inputs is provided in the present model by the powerful inhibitory input from the SNr to the SC. It is well established that neurons in the SNr maintain a high firing rate during periods of fixation and pause for some saccades (Hikosaka and Wurtz 1983a; Basso and Wurtz 2002). The set of saccades for which a particular SNr neuron pauses forms a contiguous region in visual space called the cell's response field. Neurons in the SNr strongly inhibit cells in the SC (Hikosaka and Wurtz 1983b; Karabelas and Moschovakis 1985). We hypothesize that SNr neurons project to a region in SC with spatially similar response fields (i.e., a topological arrangement) and that a coarse, Gaussian-shaped spatial tuning for saccade vectors exists in the depth of the pause of nigral activity. Neurophysiological evidence for the latter assumption exists (Basso and Wurtz 2002), but the existence of a topological projection has only been confirmed in the cat (Jiang et al. 2003). Other studies dispute the Gaussian-shaped spatial tuning of the pause in SNr saccade-related activity (Handel and Glimcher 1999, 2000; Bayer et al. 2004). Although the resolution and form of the spatial tuning of SNr neurons are still subject to debate, we will model our responses in the present model on those reported by Basso and Wurtz (2002).

In our model the pause in SNr activity disinhibits a broad region of SC and interacts with activity already induced at sites in the SC that have received recent visual inputs. The model of the SC, including spatially tuned SNr input, is initially optimized to produce accurate saccades to single visual inputs with neurophysiologically realistic SC population discharge without the use of lateral inhibitory connections in the model SC. The model uses inhibitory feedback from the brainstem to reduce discharge in the SC during a saccade. The evidence for such feedback to the SC is controversial (see Goossens and Van Opstal 2000 and Soetedjo et al. 2002 for opposing views and a summary of existing references for or against the notion of efferent feedback to the SC).

An emergent property of our model, optimized on single visual inputs, is that it produces many of the trajectory variations reported to occur in a visual search paradigm with multiple potential targets in monkeys (Arai et al. 2004) when multiple simulated visual stimuli are input to the model SC. At the same time we demonstrate that the highly curved saccade trajectories that occasionally occur with double-step or visual search paradigms (Port and Wurtz 2003; Arai et al. 2004) cannot be produced with a model that only includes the SC/SNr network. We suggest instead that an additional parallel network that has inputs at the level of the saccadic burst generators in the brainstem must exist. We first estimate the spatiotemporal form that this parallel input, acting with the model's distributed input from the SC, would need to produce accurate, straight saccades to single targets. Finally, we compute the necessary parallel input, acting with the SC, that would be required to produce highly curved saccadic trajectories. The presence of a parallel, error-sensing network, and a suggestion that it is comprised of a pathway through the cerebellar posterior vermis and caudal fastigial nucleus, has been hypothesized (Dean 1995; Quaia et al. 1999), but a novel prediction of our model is that output of the cerebellar pathway may be delayed during highly curved saccades.

2 Methods

2.1 Two-dimensional distributed saccade model

Figure 1 shows a schematic representation of our model for saccade generation when multiple visual inputs exist. The SC portion of the model is shown in black outline. This portion of the model is represented as a distributed network that receives multiple visual inputs from different locations in visual space. The SC network generates a distributed output to the horizontal and vertical saccadic burst generators (SBG horiz. and SBG vert.). The details on the horizontal and vertical SBG systems are described in the appendix. Each SBG includes a neural integrator (not shown) that connects to its respective (horizontal or vertical) plant so that the output of the model is horizontal and vertical eye position. The SBGs also produce efferent copy signals of eye displacement and velocity during saccades. The eye-displacement signals come from resettable integrators. These inhibitory signals are fed back in a distributed fashion to the SC network to reduce collicular output during saccades. Ribbon arrows represent distributed connections in Fig. 1. The SBGs also include the gating network for saccade activation produced by the omnipause neurons. We will refer to the portion of the model shown in black outline as the colliculus-only network.

The signal inputs to the SBGs shown in red are hypothesized neural inputs in parallel to the distributed input from the SC. These parallel signals are needed to explain the full operation of the saccadic system. The approach followed in the results section will be to first assume that these parallel inputs do not exist. The colliculus-only network with its feedback from the SBGs will be optimized with simulations of single-target inputs, and then we will determine

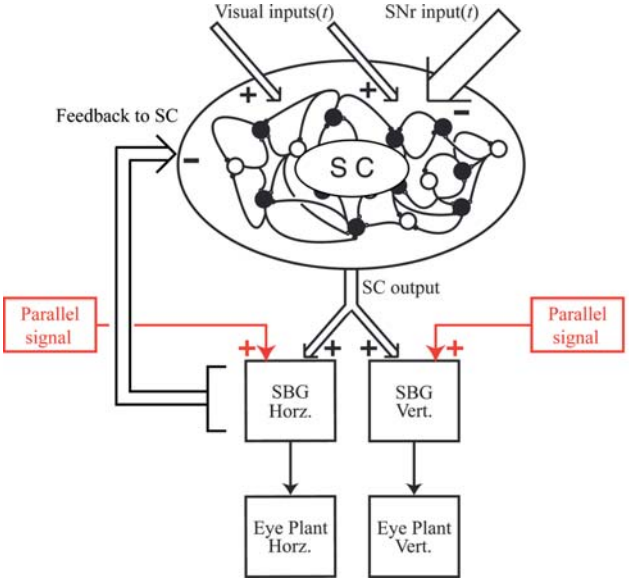

Fig. 1. Saccadic system model for multiple competing visual inputs including parallel control by distributed SC (*black outline*) and by additional parallel (*red outline*) inputs to the brainstem SBGs. The SC is a network of units with local excitatory and short-range lateral inhibitory connections. Inputs and outputs from SC are distributed (*ribbon arrows*). Spatially separated visual inputs excite multiple loci of SC activity. Spatially tuned disinhibition from the SNr interacts with visually activated loci on the SC to generate weighted input to the SBGs. In the model, the SBGs generate vertical and horizontal components of eye movements and include NIs for feedforward connections to the eye plants. Inhibitory eye-displacement signals from resettable NIs (not shown) and eye-velocity feedback to the SC from the SBGs reduce collicular output during saccades

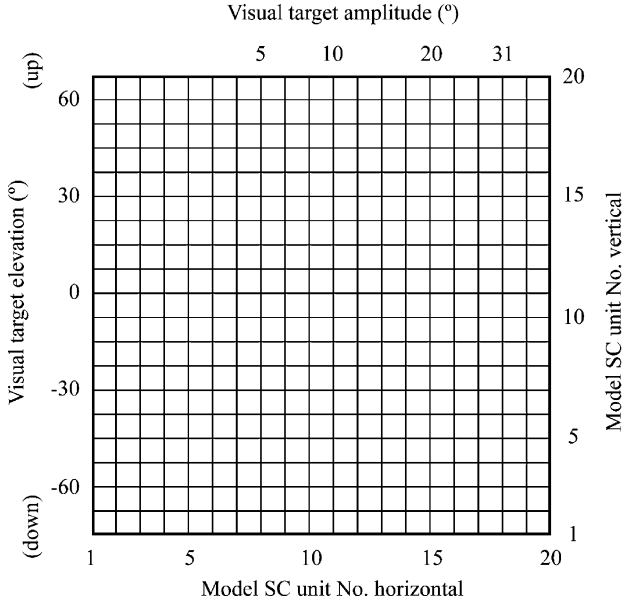

Fig. 2. The SC network is mapped onto a 20×20 grid of computational units. The corresponding representation in visual space is shown by the visual target amplitude (5–31°) and elevation (60° down to 60° up) axes. In the present model simulations, only a single, unilateral SC grid that generates contralaterally directed saccades is considered, since in this initial model SC activity will only be simulated for a two-target situation in which both targets appear in the contralateral visual hemifield

how much of the trajectory variation reported to occur when multiple potential visual targets are present can be explained by the colliculus-only model. Finally, it will be demonstrated that the colliculus-only model cannot simulate all the types of trajectory variation that occur in monkey. The necessary parallel input at the level of the SBGs, in addition to that provided by the colliculus-only model, will be computed in order to simulate these variations.

The details of the colliculus-only network have been published (Arai et al. 1999), so we provide only a brief explanation of its connectivity and operation here. The SC network shown in Fig. 2 is a 20×20-unit spatial array. This grid of laterally interconnected computational units is organized to simulate the topological relationship of neurons in the SC to the location of targets in the visual field. Location in the visual field is shown by the visual target amplitude (5–31°) and elevation (60° down to 60° up) axes. In this paper, SC activity will only be simulated for a two-stimulus situation in which both visual stimuli appear in the same hemifield. Thus, only a single SC grid that generates contralaterally directed saccades is considered. The model motor map of the SC reproduces the logarithmic compression of target amplitude found in the actual SC.

The dynamics of the interconnected SC units are described by the vector equation

$$\tau \frac{d\mathbf{x}(t)}{dt} = -\mathbf{x}(t) + \mathbf{W}\mathbf{z}(t) + \mathbf{v}(t) - \mathbf{f}_p(t) - \mathbf{f}_v(t), \quad (1)$$

$$\mathbf{z}(t) = f(\mathbf{x}(t)), \quad (2)$$

where $\mathbf{x}(t)$ approximates the activation profile and $\mathbf{z}(t)$ represents the discharge profile of each model unit. Both are arrays with 400 (20×20) elements, but for purposes of the numerical simulations they can be treated as 400 by 1 vectors; $\mathbf{W}$ is a 400×400 matrix of intracollicular connection weights, $\mathbf{v}(t)$ is the visual input, $\mathbf{f}_p(t)$ and $\mathbf{f}_v(t)$ are eye-position-displacement and velocity-feedback signals, respectively, from the brainstem, f is a component-wise nonlinear function that limits the rate of discharge in model SC units to the range 0–1.0, and τ is the membrane time constant of a SC computational unit ($\tau = 3$ ms). A brief (10-ms), spatially localized pulse input ($\mathbf{v}(t)$ in (1)) is applied to the SC to generate a saccade eye movement. This input is centered on the location corresponding to a simulated visual target and is a bivariate Gaussian in collicular space that declines in intensity isodirectionally with radial distance from its center with a standard deviation of two model units. The feedback signals ($\mathbf{f}_p(t)$ and $\mathbf{f}_v(t)$) are computed by

$$\mathbf{f}_p(t) = fb_p(t) \cdot \mathbf{r}_p, \quad (3)$$

$$\mathbf{f}_v(t) = fb_v(t) \cdot \mathbf{r}_v, \quad (4)$$

where $fb_p(t)$ and $fb_v(t)$ are, respectively, the displacement and velocity signals from the downstream structure, and the vectors $\mathbf{r}_p$ and $\mathbf{r}_v$ are the distributed feedback weights across the SC. In our previous colliculus-only model, the population discharge is driven down nearly to zero by saccade end by the feedback signals

Table 1. Parameters in the brainstem model and eye plant

Time constant (τ_1)	10 ms
Time constant (τ_2)	0.15 s
Time constant (τ_3)	5 ms
Gain (g)	1.0
Gain (k)	0.15
Scaling parameter (d_1)	1/20
Scaling parameter (d_2)	1/800
Constant (b_m)	1100
Constant (b_k)	12.4
Constant (e_0)	1.8

$$m_h(t) = \mathbf{w}_h^T \cdot \mathbf{z}(t), \tag{5}$$

$$m_v(t) = \mathbf{w}_v^T \cdot \mathbf{z}(t), \tag{6}$$

where $m_h(t)$ and $m_v(t)$ are input signals to the horizontal and vertical SBGs, $\mathbf{w}_h$ and $\mathbf{w}_v$ are, respectively, horizontal and vertical feedforward weight vectors, and T represents the transpose operation. Note that the signs (+ and −) of the input signals ($m_h(t)$ and $m_v(t)$) to the SBGs indicate right and leftward directions for the horizontal system and up and downward directions for the vertical system, respectively.

As described in the introduction, the previously optimized intracollicular connection matrix (**W**), which included local excitatory weights and extensive long-range inhibitory weights, was modified to include only short-range lateral inhibitory interconnections. The pattern of the local excitatory connections used was the same as previously reported (Arai et al. 1999). Values of the modified intracollicular connections as a function of space (distance between two units) on the SC map were set to [0.48, 0.29, 0.30, 0.05, −0.30, 0, 0, 0, 0, 0, 0] for distances between two units [0, 1, 2, 3, 4, 5, 6, 7, 8, 9, 10]. Positive and negative values represent (local) excitatory and limited (short-range lateral) inhibitory interconnections, respectively. The connection weights in the 2D SC model are radially symmetric in any direction, and weights for noninteger distances between two units are determined by interpolating the table above. This pattern of lateral weights closely resembles that determined by photostimulation techniques in a SC slice preparation (Özen et al. 2004).

In a previous paper (Arai et al. 1999) we modeled the known inhibitory input to the SC from the SNr as a global signal that was turned off just before saccade onset, leaving distributed activity in the model SC to be governed entirely by intracollicular connections and inhibitory feedback from the SBGs. In the present paper we use a more realistic representation of the perisaccadic signal input to the SC from the SNr. Figure 3 show the assumed topological arrangement of the inhibitory connections to SC from SNr. The upper flat grid (Fig. 3a) indicates that during fixation each unit in the SC grid receives an equal level of inhibition (value = 0.5) from a distributed SNr input. The Gaussian-shaped bowl shown in Fig. 3b indicates that a broadly distributed portion of the SC grid receives a much lower level of inhibition during a particular saccade

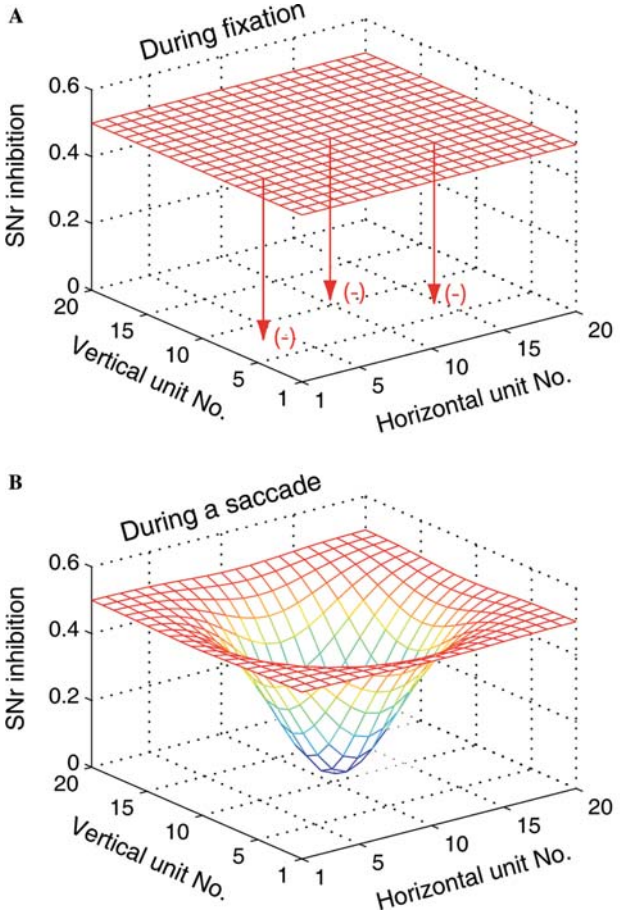

Fig. 3. Topologically organized inhibitory input to the SC motor map from the SNr during fixation (**a**) and spatially tuned disinhibition during a saccade (**b**). The visual field is represented by the 20×20 unit SC network as shown in Fig. 2 by the x–y axes. The *upper flat grid* (**a**) indicates that during fixation each unit in the SC grid receives global and constant inhibition from a distributed SNr input. The Gaussian-shaped bowl (**b**) indicates that a broadly distributed portion of the SC grid receives a much lower level of inhibition during a saccade. Distributed visual inputs that are located near the center of this bowl are greatly facilitated in comparison with those that appear closer to the edges of the bowl. In the example shown here, the maximum SNr disinhibition (the bottom of the bowl) is located at 10° horizontal (model SC horizontal unit No. 11 and vertical unit No. 11 on the SC map; see Fig. 2). See text for details of the temporal and spatial parameters of the Gaussian bowl of disinhibition

vector. In the example shown here, the coded saccade is a 10° horizontal movement. The bowl of disinhibition from the SNr is generated by the following equation:

$$I(i, j) = k1 - k2 \cdot \exp\left(-\frac{(i - x_c)^2 + (j - y_c)^2}{2\sigma^2}\right), \tag{7}$$

where $I(i, j)$ is the SNr inhibition to a SC unit at location (i, j) on the map in Fig. 2, (x_c, y_c) is the center position of the SNr disinhibition, and $k1$, $k2$, and σ are free parameters. In model simulations, these parameters, $k1$, $k2$, and σ, were set to 0.5, 0.5, and 3.5, respectively, except where noted. The value of the sigma was determined to fit to the shape of the SNr disinhibition in space (Basso and Wurtz 2002). During periods of fixation the SNr inhibitory input

to the SC grid is constant: $I(i, j) = k1 = 0.5$ for all i and j. Equation (7) specifies SNr input to the SC beginning at 20 ms before saccade onset until saccade end. The weight of the intracollicular connections are effectively reduced by shunting type inhibition (Yuille and Grzywacz 1989) from the SNr:

$$w_{(i,j)(k,l)} = \frac{w0_{(i,j)(k,l)}}{(1 + I(i, j))}, \left(if\, w0_{(i,j)(k,l)} > 0\right), \tag{8}$$

where $w_{(i,j)(k,l)}$ is the weight of the intracollicular connection from a SC unit at location (k, l) to one at location (i, j), and $w0_{(i,j)(k,l)}$ is the default value of the interconnection. In the present model, we assume that only the local excitatory interconnections ($w0_{(i,j)(k,l)} > 0$) are modulated by the SNr inhibition. Note that shunting type inhibition is not additive with excitation but instead acts to modulate excitatory input.

2.2 Parameter optimization

Model parameters were first optimized as described in Arai et al. (1999), but with the modified SNr input as described in (7) and (8) for the colliculus-only portion of the model.

Briefly, there are three sets of distributed parameters to be determined – the intracollicular connections (**W**), the feedforward ($\mathbf{w}_h$ and $\mathbf{w}_v$), and the feedback weights ($\mathbf{r}_p$ and $\mathbf{r}_v$). The intracollicular connection matrix (**W**) is set by using the lookup table described in the previous section. The feedforward and feedback weights are trained through an optimization procedure so that the model is able to produce accurate, single-target saccades. The cost functions for the horizontal and vertical saccade systems to be minimized are determined by

$$J_h(\mathbf{w}_h, \mathbf{r}_p, \mathbf{r}_v) = \frac{1}{2}\int_0^{T_1} (E_h(t) - E_{hd}(t))^2 dt, \tag{9}$$

$$J_v(\mathbf{w}_v, \mathbf{r}_p, \mathbf{r}_v) = \frac{1}{2}\int_0^{T_1} (E_v(t) - E_{vd}(t))^2 dt, \tag{10}$$

where E_h (t) and E_v (t) are, respectively, horizontal and vertical eye movements in time generated by the model, E_{hd} (t) and E_{vd} (t) are, respectively, desired horizontal and vertical eye movements, and T_1 is the time of saccade end. The feedforward and feedback weights are updated iteratively by calculating the derivative of the cost functions with respect to $\mathbf{w}_h$, $\mathbf{w}_v$, $\mathbf{r}_p$, and $\mathbf{r}_v$.

3 Results

3.1 Saccades with straight trajectories to single-target inputs

The SC feedforward and feedback weights were optimized iteratively during trials in which only single simulated visual inputs to the SC were made. Target inputs were varied from 5° to 20° in amplitude and from 45° up to 45° down. The cost function to be minimized by the optimization procedure is described in Methods. In these single-target trials we assumed that the distributed disinhibition from the SNr was centered at the same place on the SC map where the single visual input was located. In Fig. 4 we show one example of the operation of the optimized colliculus-only model when it is presented with a single visual target input (20° in amplitude and 45° up and to the right in direction). Distributed activity in the SC is centered at the location of the visual input and is greatest at saccade onset (Fig. 4b, left plot). Distributed inhibitory eye displacement and velocity feedback reduce the ensemble activity in the SC as the saccade progresses (Fig. 4b, right). The weighted, summed input at the level of the horizontal and vertical SBGs during this example saccade is shown in Fig. 4c. This plot illustrates the temporal profile of the signals required as inputs at the level of the SBGs to generate accurate saccades with realistic velocity profiles (Fig. 4d), regardless of how the signals are synthesized by upstream processing. Following the optimization procedure, saccades to any location in visual space represented on the grid (Fig. 2) were accurate. Moreover, velocity profiles during saccades resembled those recorded in the monkey in our laboratory, and the collicular population discharge closely resembled that recorded in one class of SC cell, the burst neurons (Anderson et al. 1998). However, in the monkey many SC cells continue to discharge well beyond the time of saccade end (Anderson et al. 1998; Rodgers et al. 2003). This problem will be addressed below when we compute the necessary parallel signal input needed to achieve saccade accuracy with more realistic total SC discharge.

3.2 Altered saccade trajectories in multitarget visual search paradigms

It has been shown that paradigms that create strong competition among alternative visual stimuli for the goal of a saccade produce much more saccade trajectory variability than paradigms that involve only single-target situations (Minken et al. 1993; McPeek et al. 2003; Port and Wurtz 2003; Arai et al. 2004). Figure 5 shows some example trajectories taken from unpublished data from our laboratory that illustrate this variability. A monkey performs a popout visual search task in which it is required to saccade to the location of the odd-colored target. The animal first fixates at the center of a computer monitor, a location indicated by the small cross in Fig. 5. After a random fixation interval four visual stimuli appear simultaneously and the fixation point disappears. The animal is rewarded for making a saccade to the vicinity of the odd-colored stimulus (called the target), which in all three examples shown in Fig. 5 appears at the oblique, 45° upper, position in the array. The location and color of the target were varied at random in a block of trials. On a few randomly selected trials only a single visual stimulus appeared at one of the four array locations. In these trials the animal was rewarded for making a saccade to the location of the single target. The light red contour in Fig. 5 that surrounds the stimulus in the upper-right position in the array shows the 95% confidence ellipse (Johnson and Wichern 1988)

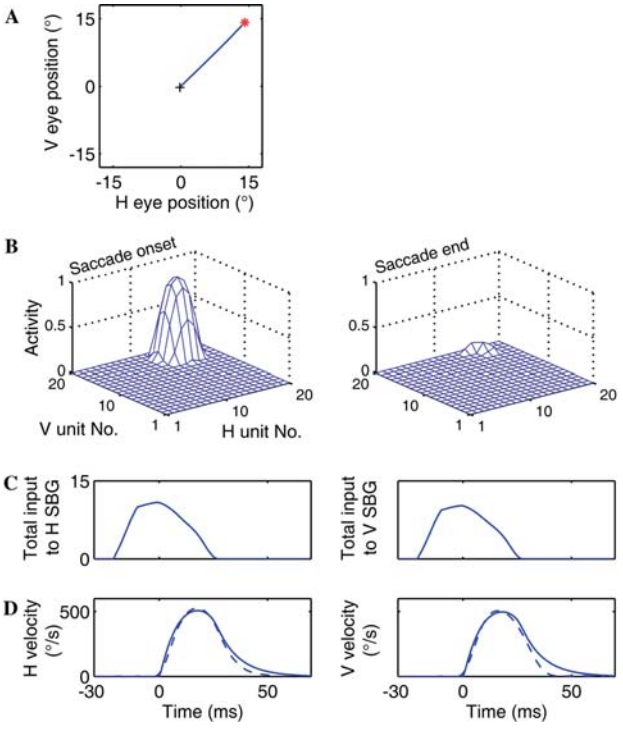

Fig. 4. Distributed activity in the optimized SC portion of the model for a 20°, 45° saccade direction up and to the right. **a** Eye movement trajectory for the saccade. Location of the single target in the visual field is shown by the *red asterisk*. Initial fixation location is shown by the *small cross*. **b** Distributed activity in the SC network (see Fig. 2 for an explanation of the grid coordinates in visual space). Activity at saccade onset is shown at the left and at saccade end at the right. **c** The summed, weighted input from the SC to the horizontal and vertical SBGs. **d** Component horizontal and vertical eye velocities produced by the model during the 20° saccade (*solid curves*) compared to average component eye velocities for the same saccade from a single monkey

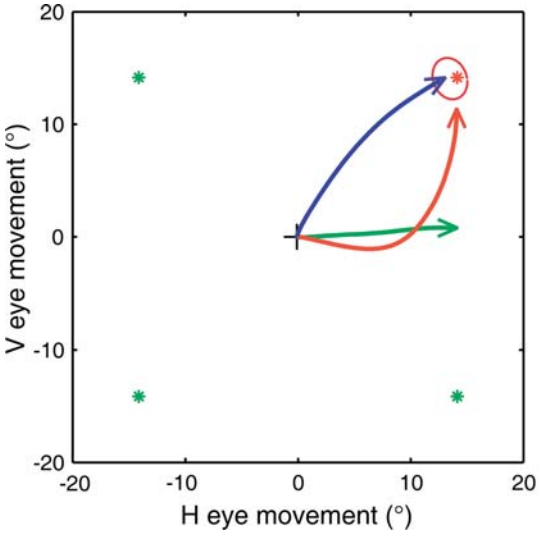

Fig. 5. Three distinctive variations of saccade trajectory produced by a monkey performing a visual search task. The *small red* and *green asterisks* represent locations of the target and three distractors, respectively. In the search task the animal was rewarded for making a saccade to the location of the odd-colored target. *1* slightly curved, on-target saccade (*blue*); *2* averaging saccade (*green*); *3* highly curved saccade (*red*). The *light red contour* around the target location shows the 95% confidence ellipse for single-target saccades made by the same animal to the upper-right target location. *Arrowheads* indicate saccade direction and endpoint

for saccade endpoints when only a single target appeared at this array location. Saccades made to the single targets (not shown) were relatively straight and generally landed within a degree or two of visual angle and amplitude from the target located at 20° of eccentricity.

On trials in which the multitarget search array appeared, saccades became more variable. The three example saccades shown in Fig. 5 illustrate particular aspects of this variability, although they were selected from a continuum of variation in trajectory. About a quarter of the saccades made in the search condition were indistinguishable from movements made during the single-target condition (not shown). That is, these saccades were relatively straight and landed inside the 95% confidence limits around the target. In contrast, approximately one third of the saccades showed a small initial direction error (blue curve) at saccade onset. This error was reduced during the saccade by curvature of the trajectory back toward the target so that the movement still landed within the 95% confidence ellipse determined from single-target behavior. About 10% of the saccades showed larger initial directional errors (green curve) and retained this directional error even at saccade end. These "averaging saccades" landed closer to the directional line bisecting the angle between the two flanking visual stimuli than to either the target or a distractor. In general, most averaging saccades were also hypometric. That is, they had amplitudes that were less than the radial eccentricity of the stimuli in the search array (20° for the data shown in Fig. 5) and thus would have been considerably hypometric to the 95% confidence ellipse for single-target saccades if their directions had been rotated into alignment with the direction of the target. Finally, on infrequent occasions large errors in initial direction were coupled with corrective curvature (the red curve in Fig. 5) during the saccade such that by the terminal phase of the saccade the instantaneous direction of the movement pointed at the target but was very different than the original direction between the fixation point and the target. Saccades with this type of trajectory have been called highly curved saccades (Minken et al. 1993; Port and Wurtz 2003). The trajectories of these saccades were normally short of the 95% confidence ellipse.

The goal of the present modeling effort was to determine if interactions between the activity generated by visual inputs to the SC motor map and the spatially tuned disinhibition from the SNr to this same map could produce each of these experimentally observed extremes of trajectory variation (Fig. 5) in simulated visual search trials.

After the optimization procedure discussed above was completed, the interconnections within the simulated SC map, the distributed feedforward connections to the horizontal and vertical saccadic burst generators, and the feedback connections to the SC were frozen. Next, two identical visual inputs in the same visual hemifield were

simultaneously input to the model SC. The subsequent distributed spatiotemporal activity on the SC map now depended on what assumptions were made about the nature of the SNr disinhibition. Without long-range lateral inhibitory connections in the model SC, there was no competition between the two visually activated regions of the SC map and both loci of activity would persist until saccade initiation. A logical assumption is that SNr disinhibition remained unimodal and was centered at the location of one of the visual stimuli. When the location of the SNr disinhibition matched that of the visual target in the upper-right field, the subsequent trajectory was similar to that when only a single target appeared at this location. The interaction of activity induced by the visual stimulus at this location and with the greater level of disinhibition of the same region of the map produced an initial saccade direction that was close to the direction of the upper visual stimulus. We will refer to this location as the "target." The locus of activity at the SC site that codes the location of the lower visual stimulus was rapidly quenched because it was located far from the center of the SNr disinhibition. The saccade trajectory went directly to the location of the target and was not noticeably different than that when a single visual stimulus appeared at this location.

3.3 Slightly curved saccades

A more interesting case occurs when two visual stimuli are input to the SC map and we assume that, like the SC, the distribution of activity modulation in the SNr is not winner-take-all but instead shows weighted bowls of disinhibition at the locations of both visual stimuli. This situation is quantified by:

$$I(i,j) = k1 - \alpha \cdot k2 \cdot \exp\left(-\frac{(i-x1_c)^2 + (j-y1_c)^2}{2\sigma^2}\right) - \beta \cdot k2 \cdot \exp\left(-\frac{(i-x2_c)^2 + (j-y2_c)^2}{2\sigma^2}\right), \quad (11)$$

where $(x1_c, y1_c)$ and $(x2_c, y2_c)$ are the center positions of two SNr disinhibition bowls, and α and β are weight parameters ($0 \le \alpha \le 1.0$, $0 \le \beta \le 1.0$). An example of a saccade that results in the situation governed by (11) is shown in Fig. 6. In this case the deepest bowl of disinhibition is located at the target (upper visual stimulus). We indicate the degree of disinhibition by the color of the circular icons in Fig. 6a, with dark blue being the deepest level and yellow the more shallow. The spatial locations of the two minima of disinhibition are shown by the centers of the circular icons. The actual distributed map of disinhibition is shown in Fig. 6b using the same color coding to indicate the depth of disinhibition. Note that SNr disinhibition is very broadly tuned and affects almost the entire visual hemisphere coded in the SC model. This widely distributed disinhibition of the SC map is established 20 ms before saccade onset in the model simulations and remains static for the duration of the saccade. In this simulation the two visual stimuli, $(x1_c, y1_c)$ and $(x2_c, y2_c)$, are located at (H15, V17) and (H15, V5), respectively, which correspond to the center locations of two visual stimuli at 20° in amplitude and ±45° in direction. For the simulation shown in Fig. 6b, the weight parameters, α and β, are set to 1.0 and 0.3, respectively.

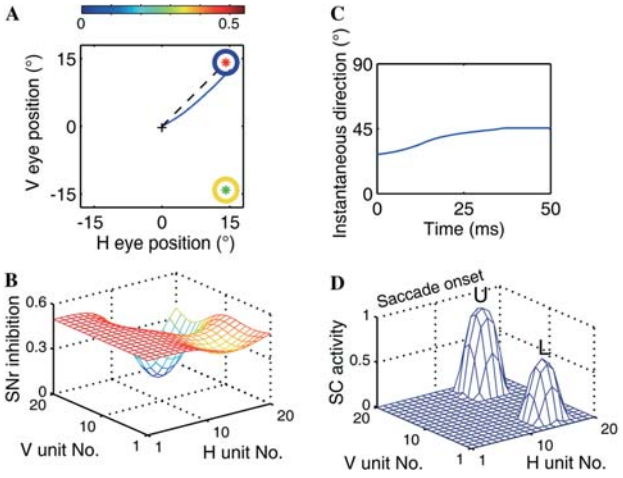

Fig. 6. Distributed activity for a simulated slightly curved saccade. **a** Simulated saccade trajectory (*solid blue curve*) when two competing visual stimuli appear in the right visual hemifield. The *small red* and *green asterisks* represent the target and a distractor, which are located at 20° in amplitude and ±45° in direction. A straight saccade trajectory to a single target located at the upper-right stimulus location is shown for comparison (*dashed black line*). The visual stimuli produce two basins of disinhibition in the SNr modulation of the SC. The *blue annulus* shows the center of the distributed disinhibition surrounding the upper visual stimulus. The *yellow annulus* shows the center of disinhibition around the lower visual stimulus. The level of inhibitory input to the SC from the SNr is color coded (see scale above **a**). *Blue* indicates a complete removal of SNr inhibition. Because the upper stimulus has been selected as the target, its basin of disinhibition is deeper, as can be seen in more detail in **b** (from (11), $\alpha = 1.0$ and $\beta = 0.3$). The same color code (**a**) for inhibition is used in this panel. **c** Instantaneous direction of saccade trajectory. Saccade onset is at zero time. **d** Distributed activity in model SC map at saccade onset. U = corresponds to SC activity at the site representing the stimulus in the upper visual field. L = activity at the site representing the stimulus in the lower field

The arrangement of SNr disinhibition shown in Fig. 6 greatly favors the upper target, but not as strongly as when it is unimodal and located only at the upper target. Figure 6d shows that some activity remains at the lower visual stimulus site at the time of saccade onset. Due to the vector-summation nature of the model connections to the SBGs ((5) and (6)), the remaining activity at the lower site causes the initial direction of the saccade to be inclined below the direction of the target (Fig. 6c). This directional error is reduced gradually by dynamic interactions between the activity generated by the intracollicular connections and the distributed disinhibition from the SNr as the saccade progresses and activity at the lower mound is rapidly extinguished. This change in saccade direction produces a trajectory that curves somewhat back toward the direction of the target like the actual saccade shown in blue in Fig. 5.

In summary, varying the relative depths of disinhibition from the SNr at the sites of multiple visual stimulation in the SC map produces various amounts of subsequent saccade curvature. The initial saccade direction is inclined slightly away from the final target, but the trajectory curves

partially back toward the stimulus with the deeper basin of disinhibition. The process may represent the adjustment of saliency of various collicular loci of visual activity by basal ganglion inputs.

3.4 Averaging saccades

A representative averaging saccade trajectory made by a monkey is shown by the green curve in Fig. 5. This trajectory is completed at a location near the line bisecting the angle between the two visual stimuli; however, everything that we describe in this section is also reproduced by the model for trajectories that end anywhere between the locations of the two visual stimuli. Figure 7 illustrates what happens to a saccade trajectory when two identical visual stimuli are applied to the model at the upper and lower locations and two identical basins of the nigral disinhibition are located at the sites of the two visual stimuli. Because neither stimulus has been selected as the target, the depth of disinhibition is the same at both visual stimulus locations and the weight parameters are set to values less than 1.0 ($\alpha = \beta = 0.5$ in Fig. 7b). In this case neither mound of visually induced SC activity is placed in a privileged position, but instead, both are reduced in amplitude by equal amounts at saccade onset in comparison to that seen when the full disinhibition is located at one of the mounds (compare Figs. 4b and 7d). The initial saccade direction is pointed midway between the two basins of the nigral disinhibition, even though little or no activity appears at this location on the SC map. As the saccade progresses, both mounds are reduced at the same rate by the negative feedback of eye-displacement and eye-velocity signals to the SC map. The symmetry of the distributed activity on the SC map keeps the saccade direction constant throughout the movement. The movement ends at a location that is on the direction line between the initial eye position and the midpoint between the two visual stimuli but is clearly hypometric in amplitude, as was the actual monkey averaging saccade shown in Fig. 5. Hypometric end positions frequently accompany averaging behavior in both monkeys and humans when saccades are made in a visual search paradigm (McPeek et al. 2000; Arai et al. 2004).

The production of hypometric saccades in the model seems to be counterintuitive in view of the fact that our model uses weighted vector summation of SC inputs to the brainstem portion of the model ((5) and (6)). It might be expected that more total activity would be present on the SC map when averaging behavior with multiple visual stimuli occurs than would be present if a single target were instead placed at the midway point between the two visually induced mounds of activity. It is clear in the two-visual-stimuli condition (Fig. 7) that the up- and down-drive signals conflict and cancel at the level of the vertical burst generator in the brainstem portion of the model. On the other hand, both of the horizontal commands generated by the activity at the two locations on the map produce rightward command signals. How is it possible to use vector summation to compute the drive of these two distributed signals and still have hypometric behavior?

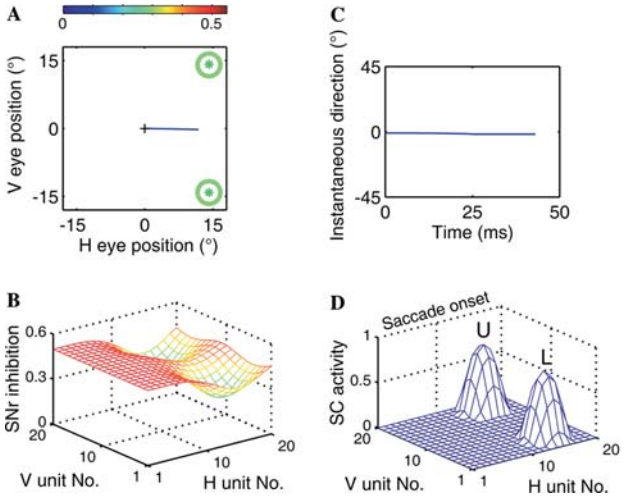

Fig. 7. Distributed activity in the model SC for a simulated averaging saccade. **a** Saccade trajectory is shown by the *blue line*. Two visual stimuli (*green asterisks*) are input at 20° in amplitude and ±45° in direction. The centers of the basins of disinhibition from the SNr are shown by the *green annuli*. Because neither stimulus has been selected as the target, the depth of disinhibition is the same at both visual stimulus locations ($\alpha = \beta = 0.5$). Inhibition color is coded as in Fig. 6. **b** Details of the distributed SNr input to the SC map. **c** Instantaneous direction of the saccade. **d** Activity on the model SC map at saccade onset is shown in the same format as in Fig. 6

We have pointed out that the activity in each of the two mounds of discharge on the map is smaller than that produced by a single target located at the same eccentricity. This effect has already been described by Van Opstal and Van Gisbergen (1989), but in their model long-range lateral inhibitory connections in SC produced the reduction (normalization) of SC activity. Since such long-range inhibitory connections may not exist (Özen et al. 2004), we hypothesize in our model that it is the weighted, distributed SNr disinhibition that produces the reduction of SC output. In addition, one needs to consider the effect of the eye-displacement and velocity-feedback signals to the SC map. In our previous paper we described how the weights connecting this feedback signal to the SC motor map in the model vary in value with larger values connected to rostral and smaller values to caudal locations (Arai et al. 1999). The presence of this pattern of distributed feedback helps to produce shorter duration activity (hence, smaller saccades) when visually evoked activity is located in the rostral SC. This behavior has been confirmed in single-unit recordings in the monkey SC (Waitzman et al. 1991; Anderson et al. 1998). Sites in SC at a given rostral/caudal meridian (coding saccades of fixed amplitude) tend to have their activity driven down during saccades by feedback at a rate that is fixed for that degree of eccentricity. When two mounds of activity at the same eccentricity are present whose combined discharge would potentially produce a faster movement, the increased eye-velocity feedback drives both mounds down more quickly, thus stabilizing an invariant size of movement for variable amounts of activity at the same SC meridian. The two effects together (high levels of remaining nigral inhibition at

the target sites and eye-velocity feedback to the SC) produce the emergent and unexpected result in the model that averaging saccades made to locations in between visually generated mounds of activity are hypometric in the model, which fits the experimental observations cited above.

3.5 Highly curved saccades

Thus far we have been able to simulate some of the types of saccadic trajectory variability that have been reported to occur when multiple visual stimuli compete for the goal of a saccade. We now turn our attention to the third type of trajectory variation shown in Fig. 5, the highly curved saccade (red curve). The colliculus-only model simulation for this case is shown in Fig. 8. Two visual stimuli are applied to the model simultaneously as before, but the depth of disinhibition is initially deeper at the location of the lower visual stimulus (green asterisks, $\alpha = 0.3$ and $\beta = 1.0$). At saccade onset the lower mound of activity is favored and the activity in the upper mound is reduced in comparison to that present in the lower mound. The initial saccade direction is biased toward the location of the lower stimulus, as expected. Soon after the saccade begins (at 4 ms after saccade onset), we assume that the nigral decision has been altered and the upper stimulus has now been selected as the goal. The position of the deeper basin of SNr disinhibition is switched to be located at the position where the upper visual stimulus was applied (α and β are switched simultaneously to 1.0 and 0.3, respectively). This switch causes the lower mound to become disadvantaged with respect to the upper mound, and its ensemble activity begins to decline rapidly. This behavior is shown more clearly in Fig. 8e. Here we plot the activity of the most active unit in the SC motor map in each mound of activity as a function of time from before saccade onset to saccade end. Figure 8e shows that activity peaks first at the lower location on the map (green curve), as the saccade direction is into the lower hemifield. Activity at the lower location on the map declines rapidly as the activity begins to increase at the upper site due to the spatial switch of the dominant nigral disinhibition. At this time the trajectory begins to rotate upward. Activity at the upper site then peaks and begins to decline (red curve in Fig. 8e). This sequential peaking of SC activity at different locations on the SC map during highly curved saccades fits the experimental observations made with simultaneous two-electrode recordings in the monkey (Port and Wurtz 2003).

The trajectory, however, never curves enough in the upward direction to make it point at the target by saccade end, a behavior that is at odds with that seen in monkey highly curved saccades (red curve in Fig. 5). Instead, the terminal trajectory in our simulation is in the direction coded by the original retinotopic location of the upper mound of activity (in visual space). After some reflection, it is clear that this is expected. Our distributed motor map of the SC specifies a movement direction in retinotopic coordinates. It also serves as a crude controller of saccade amplitude through the eye-velocity and eye-displacement feedback it receives, but it does not compute either component (direction or amplitude) of a vector motor error

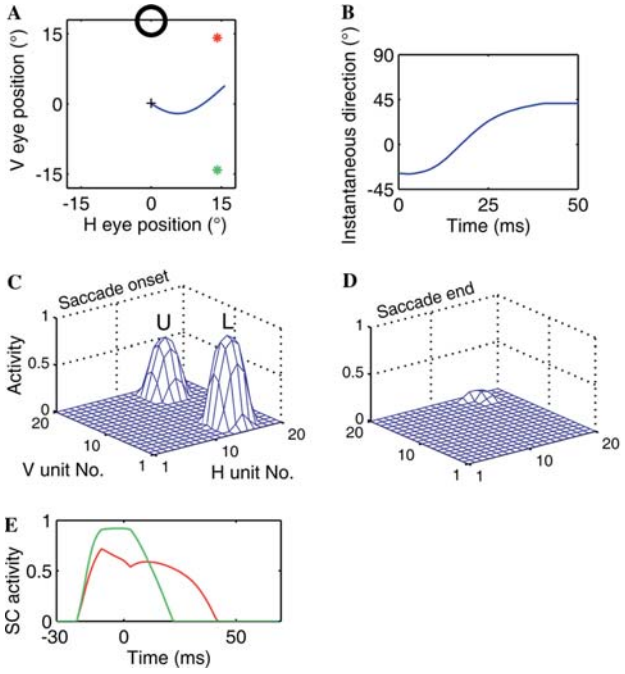

Fig. 8. Distributed activity in the model SC in attempt to simulate a highly curved saccade. **a** Two visual stimuli are applied to the same locations as in the previous simulations, but the depth of disinhibition is initially deeper at the location of the lower stimulus. Under this initial condition, the activity on the SC map centered at the lower visual stimulus is favored. The initial saccade direction is slightly downward as shown in *b*. After 4 ms following saccade onset, the position of the deeper basin of SNr disinhibition is switched to be located at the position where the actual target (upper visual stimulus) was applied (α is switched from 0.3 to 1.0 and β is switched from 1.0 to 0.3 simultaneously). After this switch, activity at the lower site begins to decline and activity at the upper site starts to increase. This causes the saccade trajectory to turn upward, but note that it never approaches the nearly pure up trajectory seen in the monkey highly curved saccade (*red* trajectory in Fig. 5). The *black annulus* represents the location of the activity on the SC map needed to drive saccades in the pure up direction. **c** Corresponding activity on SC map at saccade onset. **d** SC activity in model at saccade end. **e** Discharge of SC unit that is the most active on the map (unit H15, V5 in Fig. 2) at saccade onset time (zero on the time axis) is shown by the *green curve*. The discharge of the SC unit that is the most active on the map (unit H15, V17) at 25 ms after saccade onset is shown by the *red curve*

signal, as can be seen from the amplitude (Fig. 7) or directional (Figs. 7 and 8) errors present at saccade end.

An examination of the results shown in Fig. 8e reveals that activity reaches a peak value at the upper site at about the same time that activity at the lower site has already been largely quenched. The residue of activity at the upper site continues to direct the saccade with a final direction of about +45°. The saccade terminates with both an amplitude and direction error. One way to modify our model to better resemble the trajectory seen in the behavioral results (Fig. 5, red curve) would be to evoke a mechanism that updated the SC motor map activity to reflect the change in eye position that has occurred as a result of the first portion of the saccade trajectory. Some neurophysiological evidence exists that updating does occur in the SC map

(Walker et al. 1995), but this has only been shown for the case of two separate saccades in which the map is updated as a result of the eye-position change in the first saccade.

Two models have already simulated how this updating might be implemented in the SC for two separate saccades (Droulez and Berthoz 1991; Bozis and Moschovakis 1998). For the highly curved saccade trajectories there are never two separate saccades, but rather a single smooth trajectory. If the updating did occur in these curved single saccades, one would expect activity to occur at the site (indicated by the black annulus in Fig. 8a) in the map coding an upward direction in visual space. Port and Wurtz (2003) have recorded single cells at equivalent locations in the monkey SC during highly curved saccades and report that no significant activity appears at this site. We have not been able to generate the upward trajectories seen in highly curved trajectories with any manipulations of our SC/SNr model. For example, if the nigral disinhibition were shifted to the straight up location in visual space during the terminal phase of the movement (simulating updating at the level of the SNr), there would still be no significant activity induced at this location because the generation of activity on the map is dependent on an interaction of the ensemble activity generated by a visual stimulus with the disinhibition from the nigra. Since no visual stimulus has ever appeared at the necessary upward location, no activity would appear there even if the SNr disinhibition were shifted there.

We conclude from the results obtained in trying to simulate highly curved saccades that our simple colliculus-only model is inadequate to explain all of the variability seen in saccade trajectory in visual search paradigms. Nevertheless, it serves as an introduction to how spatially distributed visual and disinhibitory inputs can interact in a dynamic motor map and produce some trajectory variation without using strong, long-range lateral inhibitory connections that make the map too strongly winner-take-all to fit observed neural recordings in the SC.

3.6 An additional parallel input at the SBGs

Dean (1995) and Quaia et al. (1999) have proposed saccadic system models for single-target situations in which parallel drive signals from the SC and a region of the deep cerebellar nuclei, the caudal fastigial nucleus (cFN), jointly control saccades. In Fig. 1 we indicate with red lines where in our model we believe that this hypothesized parallel input would connect.

There have been no neural recordings made in the cFN in multitarget situations or during the altered saccade trajectories produced by multiple visual target competition. However, the cerebellar portion of the model of Quaia et al. (1999) requires that only a single saccadic goal be selected, and this goal is represented by activity at a specific spatial location in the contralateral cFN at saccade onset. Activity then spreads across the cFN as the saccade proceeds until the activity has shifted to a mirror image location in the ipsilateral cFN at saccade end. The rate of the spread in cFN activity is controlled by eye-velocity feedback from the SBG. It is difficult to see how multiple targets and target selection could be represented in this scheme of spreading activity. Until further recordings are made in the monkey cFN during the presentation of multiple targets and the production of altered trajectories it will not be possible to offer specific alternative mechanisms in the cerebellum that could contribute to the generation of the parallel input signal at the level of the SBGs. However, we can compute the spatiotemporal form of the parallel signal needed to generate highly curved saccades, assuming that the collicular-only portion of our model is realistic. This approach has the advantage of producing predictions about the form of the output activity of the cFN. These predictions can be used to guide future neural recordings in the monkey cFN during highly curved saccades.

We made two changes in the SC portion of the model before computing the predicted parallel signals that would be required to produce realistic straight and curved saccade trajectories. Bilateral lesions of the cFN render saccades hypermetric (Robinson et al. 1993; Takagi et al. 1998). In addition, cells identified as projecting out of the SC into the region of the saccadic burst generators continue to discharge well after saccade end (Rodgers et al. 2003). In order to assimilate these experimentally observed features into our model, the values of the distributed feedback signals to the SC map ($\mathbf{r}_p$ and $\mathbf{r}_v$) were lowered. Since the feedback signals to the SC map are assumed to be inhibitory, reduction in their values has the effect of prolonging SC discharge and making the saccades produced by the colliculus-only model hypermetric. Bilateral lesions of the cFN also reduce the initial acceleration of the eyes, and peak velocities of saccades are lowered (Robinson et al. 1993). To simulate this effect, all the feedforward weights ($\mathbf{w}_h$ and $\mathbf{w}_v$) from the SC to the SBGs were decreased.

The quantitative changes made in $\mathbf{r}_p$, $\mathbf{r}_v$, $\mathbf{w}_h$, and $\mathbf{w}_v$ were determined by an iterative procedure that lowered the feedback and feedforward vectors until the amount of saccadic hypermetria matched the average amount of hypermetricity reported by Robinson et al. (1993) in monkeys following bilateral cFN lesions and the component peak velocities were lowered by the same amount as the peak velocity decreases reported in the same study. The optimized global reduction in feedback weights was 30%, and the optimized global reduction in feedforward weights was 40%.

The plate on the left in Fig. 9a shows a spatial plot of a saccade made by the colliculus-only model to the same single-target location that was used to generate Fig. 4 (20° amplitude, 45° direction up and to the right), but now after making the two changes discussed above in the colliculus-only portion of the model. In this simulation we assumed that no parallel inputs at the level of the SBGs were present. The saccade is hypermetric by 30%. Figure 9b shows the horizontal and vertical components of the change in eye position during this hypermetric saccade superimposed on the target component positions (dashed horizontal lines) and the summed, weighted output from the SC to the horizontal and vertical SBGs (red curves). These

records show that both components of eye position were hypermetric, and comparison to Fig. 4c shows that the hypermetricity was caused by a prolonged ensemble discharge from the SC. Figure 9c compares the eye-velocity components produced by the colliculus-only model during this hypermetric saccade (solid curves) to those produced by the original colliculus model from Fig. 4d (dashed curves). The initial eye accelerations are low, and the peak velocities are about 15% low due to an insufficient ensemble input from the SC. We computed the necessary parallel signals that needed to be added to the input signals from the SC (Fig. 9b) to produce the correct total signal into the SBGs that was obtained from the data shown in Fig. 4c:

$$p_h(t) = m_h(t) - m'_h(t), \tag{12}$$

$$p_v(t) = m_v(t) - m'_v(t), \tag{13}$$

where $p_h(t)$ and $p_v(t)$ are, respectively, the horizontal and vertical parallel signals and $m'_h(t)$ and $m'_v(t)$ are the summed, weighted output from the SC with the reduced feedforward and feedback weights. The computed parallel signals are shown in Fig. 9d. The form of these signals is very similar to that of the signals provided by the cFN to the SBG in the models proposed by Dean (1995) and Quaia et al. (1999). Figure 9d shows that there is additional positive input from the parallel pathway into both horizontal and vertical SBGs at saccade onset. This is followed by smaller negative going parallel inputs to both SBGs as the saccade is terminated. With our implementation of the bilateral and up/down burst generators (see appendix) the early positive signal would provide additional excitation to the SBGs during the initial phase of the saccade. The later negative going signal would provide inhibition that cancels the remaining input from the SC near saccade termination. Figures 9e and 9a (right) show that when the input from the SC (Fig. 9b) and the parallel signals shown in Fig. 9d are combined, the model produces orthometric saccades. Figure 9f shows that these saccades have realistic eye-velocity profiles.

A similar procedure was used to compute the required parallel signal into the SBGs to produce highly curved saccades. The changes made in the colliculus-only portion of the model that produced normal saccades to single-target inputs shown in Fig. 9 were retained. In Fig. 10 we show the results of rerunning the simulation for the same two-visual-stimuli configuration used in Fig. 8. Initially at saccade onset, the nigral disinhibition favors the lower target so that initial saccade direction is down and to the right (Fig. 10a and b). At 4 ms after saccade onset the target selection process from the nigra reverses the relative depths of the disinhibition basins at the upper and lower sites, as explained in the simulation for Fig. 8. An upward-directed spatial shift in population activity in the SC takes place over time (Fig. 10c and d), as previously seen in Fig. 8 for the colliculus-only model.

We estimated the necessary parallel signals required to produce the late upward curvature of saccade trajectory seen in the actual saccade. This procedure is simplified by the following observation. Figure 10e shows the horizontal and vertical components of velocity of a

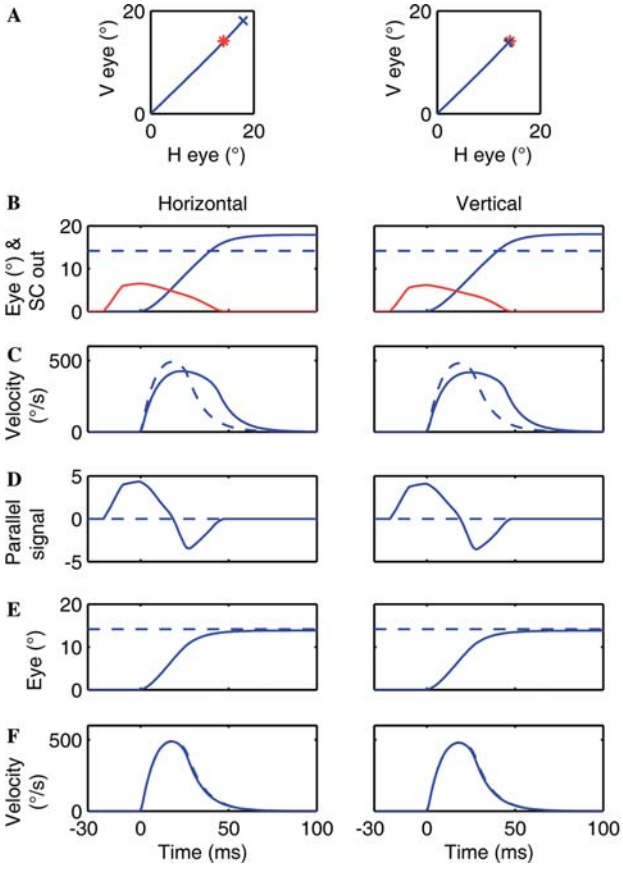

Fig. 9. Model behavior after decreasing feedforward and feedback weights. **a** A spatial plot of a saccade to a single target generated by the colliculus-only model with the reduced feedforward and feedback weights (*left panel*) and one produced by the full model including the parallel inputs (*right panel*). The target (*red asterisk*) is located at 20° in amplitude and 45° up and to the right in direction. **b** For the colliculus-only model the horizontal and vertical components of the change in eye position during the hypermetric saccade (*blue curves*), the horizontal and vertical target positions (*dashed horizontal lines*), and the summed, weighted output from the SC to the horizontal and vertical SBGs (*red curves*) are superimposed. **c** The eye-velocity components produced by the colliculus-only model during the hypermetric saccade (*solid curves*) and those produced by the original model from Fig. 4d (*dashed curves*). **d** The computed horizontal and vertical parallel signals. **e** Horizontal and vertical components of a saccade produced by full model with parallel signals from D. **f** Eye-velocity components produced by full model (*solid curves*) and those produced by original model from Fig. 4d (*dashed curves*)

simulated highly curved saccade produced by the colliculus-only model with the reduced feedforward and feedback weights (solid curves) and those of the actual highly curved saccade (dashed curves) in the monkey (Fig. 5). By comparing both velocity components, we found that for the horizontal SBG an excitatory input was needed for about 20 ms after the saccade onset and an inhibitory input was needed after the excitatory input. For the vertical SBG the necessary parallel signal is excitatory from around 5–40 ms and inhibitory from 40 to 70 ms. Based on these observations, we estimated the parallel signals as shown in Fig. 10f, in which the horizontal parallel signal

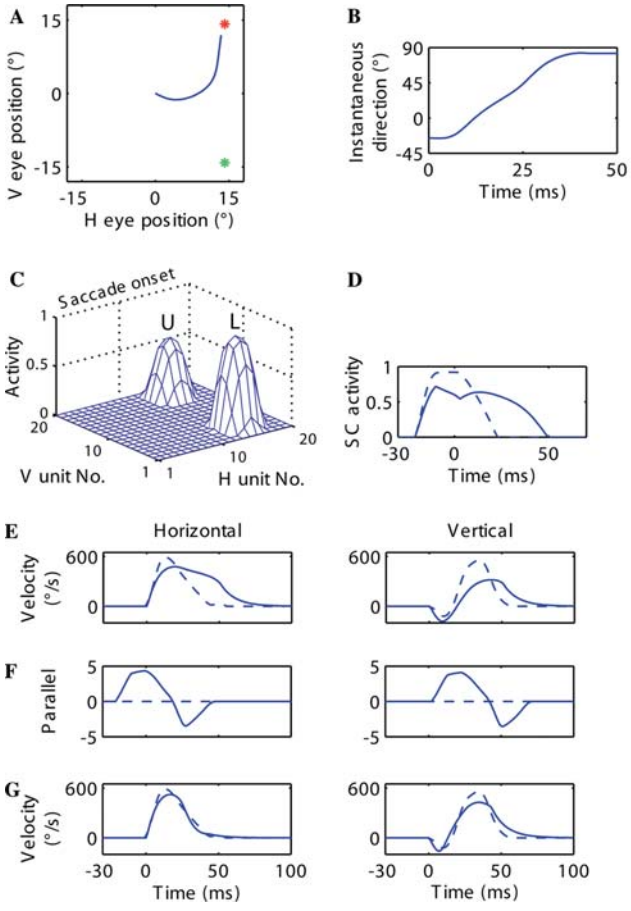

Fig. 10. Highly curved saccade generated by the full saccade model. **a** Locations of two visual stimuli (*red and green asterisks*) and two basins of the SNr disinhibition (not shown) are identical to the simulation in Fig. 8. The same timing of switching the deeper basin of SNr disinhibition from the lower to the upper visual stimulus is also used here. **b** Instantaneous direction of the saccade trajectory. **c** Corresponding activity on the SC map at saccade onset. **d** Discharge of most active model SC units in time at upper (*solid*) and lower (*dashed*) sites. **e** Horizontal and vertical components of velocity of a simulated highly curved saccade produced by colliculus-only model with reduced feedforward and feedback weights (*solid curves*) and those of actual highly curved saccade in monkey (*dashed curves*). **f** Computed horizontal and vertical parallel signals required to produce highly curved saccade whose trajectory direction points at target at saccade end. **g** Eye-velocity components produced in model by combination of parallel signals and SC output (*solid curves*). Actual component velocities in monkey during highly curved saccade repeated from **e** (*dashed curve*)

is the same as one used for the single-target case shown in the left panel in Fig. 9d and the vertical signal is delayed in time by 23 ms. Finally, the eye-velocity components produced by the combination of these parallel signals and the SC input are shown in Fig. 10g.

Figure 11 shows that a similar procedure can be applied to produce the variety of highly curved saccade that we found in a sample of saccades in the monkey. The actual saccade trajectories are shown in Fig. 11a. Figure 11b shows a family of curved saccades produced by the full model. To produce these varied simulated

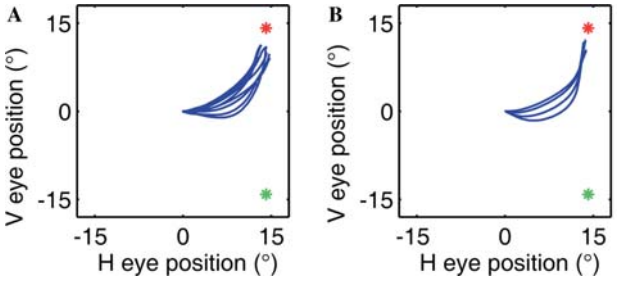

Fig. 11. A family of highly curved saccades. **a** Highly curved saccades measured in a monkey during a visual search task. **b** Curved saccades produced by full model with variable delays (10, 15, 20, and 25 ms) at onset of signal in vertical parallel channel. The locations of two visual stimuli (*red and green asterisks*) are identical to the simulation in Fig. 10

saccade trajectories, we only varied the delay (10, 15, 20, and 25 ms) at the onset of the vertical parallel signal. After the variable delay period the same signals used in the simulation shown in Fig. 10 were used for each of the trajectories. The trajectories produced by the assumption of a variable trial-to-trial delay in processing through the parallel channels produces some of the key features present in the actual saccade trajectories. The initial direction appears to be rather straight and aimed in a direction that is near the spatial average of the initial activity on the SC. The trajectory then curves after a delay into a direction that is more upward than can be produced by the colliculus-only model. The final direction and endpoint of the curved saccades are more variable than can be produced by our simple assumption of the form of the parallel signals. Nevertheless, we believe the form of the initial portions of trajectories in the simulations are realistic enough to support our main new prediction that generation of the parallel signal may be delayed in multitarget situations in comparison to the signal generated by the SC.

4 Discussion

In this report we propose a new model of the saccadic system that allows simulation of the eye movements that occur when multiple visual stimuli are present and compete as the goal for a saccade. The simulations conducted with the model explore some general issues that surface in considerations of the neural processing in distributed visuomotor maps. The competitive processes that occur in such neural maps between multiple visual inputs leading to target selection and a particular saccadic movement have been the subject of a great deal of interest recently (Schall and Thompson 1999). While we limit our current exploration of distributed networks to the SC, many of our suggestive findings could also apply to cortical visuomotor maps that are present in the frontal eye fields (FEFs).

In the past it has generally been assumed that the competitive processes that underlie target selection in such distributed visuomotor maps are governed by extensive lateral inhibitory connections between locations in the map. This pattern of connections leads to two types of ensemble behavior. In one type, called winner-take-all

behavior, one location of active neurons representing the most salient potential target emerges as the only active location on the map, and these active neurons code the direction and amplitude of the following saccade (Koch and Ullman 1985). In the other type of behavior, in which two targets are equally salient, the strong lateral connections mutually inhibit activity at the two target locations. Models of this behavior predict that the highest level of activity would appear in between the locations of two visual inputs (Van Opstal and Van Gisbergen 1989; Arai et al. 1994; Bozis and Moschovakis 1998).

The former type of behavior seems appropriate for the SC, in particular because it connects directly to the final saccade, generating brainstem circuits that we call the saccadic burst generators (SBGs). However, recent neurophysiological experiments raise doubts that the SC always operates in a winner-take-all fashion (McPeek and Keller 2002a; McPeek et al. 2003; Port and Wurtz 2003). Recordings made in the SC during averaging saccades produced by two equally salient targets in monkeys do not support the second prediction (Edelman and Keller 1998). Rather, the activity remains localized at the locations of the visual stimuli and little activity appears at the location between stimuli that represents the vector of the actual averaging saccade that is made. In addition, we have shown that it is difficult to produce curved saccade trajectories with distributed maps with strong lateral inhibitory connections because such maps tend to produce one locus of activity by the time of saccade onset (Badler and Keller 2002). Finally, studies in slice preparations suggest that long-range lateral inhibitory connections may not exist in the SC (Özen et al. 2004). Nevertheless, extracellular stimulation and recording experiments in the SC have led to the generally accepted view that long-range inhibitory connections exist in this structure (Munoz and Istvan 1998).

Although the question of the existence of inhibitory lateral connections in the SC remains unsettled, in the present model we assume that they do not exist. Instead, we use topologically organized connections and spatially tuned disinhibition from the SNr to the distributed SC map to shape the perisaccadic spatiotemporal pattern of discharge on the map. We hope that our model will spur further experimental investigation into the distributed nature of SNr modulation of SC output and into the nature of lateral interconnections in the SC.

4.1 Trajectory curvature

Curved trajectories have been produced in simulations using a distributed motor map in the cerebellum (Quaia et al. 1999). In that model a moving wave of activity in the cerebellum was posited that was driven by eye-velocity feedback. This activity in parallel with directional drive signals from the SC was used to control saccade trajectory. Initial directional errors were corrected by the time of saccade end by trajectory curvature as a result of the action of the hypothesized error-sensing cerebellar circuit. However, in this model it is not clear how the original directional errors were produced. In our model we suggest explicit distributed mechanisms involving unresolved competition among stimulus locations in the SC as the source of initial deviation away from the desired target. In the Quaia model no directional change could be produced by the SC portion of the model, but neural recordings made in the monkey SC during curved saccade trajectories do show dynamic spatiotemporal variations (McPeek et al. 2003; Port and Wurtz 2003) that resemble those produced by our colliculus-only simulations. However, our simulations showed that only a limited curvature of saccade trajectory could be produced by our hypothesized mechanism of interaction between excitatory visual inputs to the SC and spatially tuned disinhibition from the SNr. The production of highly curved trajectories that point in the direction of the target by saccade end required additional parallel inputs below the level of the SC.

4.2 Role of SNr/SC interactions in saccade trajectory variability

Other models with distributed representations of SC processing have appeared, but ours is unique in suggesting a role for spatially tuned SNr inputs to the SC motor map (Basso and Wurtz 2002). Disinhibition of the SC by the SNr input is a well-known feature of collicular function (Hikosaka and Wurtz 1983b; Karabelas and Moschovakis 1985). However, it might be argued that the spatial tuning of the SNr disinhibition is too coarse to operate in the manner hypothesized in the present model. The neurophysiological evidence for tuning in this input is contradictory. The best-tuned SNr units reported by Basso and Wurtz (2002) show a resemblance to our hypothesized tuning function for single-target inputs (Fig. 3), but the evidence from others is less convincing (Hikosaka and Wurtz 1983a; Handel and Glimcher 1999).

In the model simulations shown in Figs. 6–10, the parameter of the SNr spatial tuning function, σ, in (7) and (11) was set to 3.5. To explore how broadening the tuning functions for SNr disinhibition would effect the predictions of our model, we increased σ to 6.0, and the feedforward weights from the SC model to the SBGs were reoptimized using single visual targets to generate accurate saccades. After the reoptimization, two visual stimuli were applied simultaneously to locations at 20° in amplitude and ±45° in direction to the SC map, and the same SNr patterns of disinhibition as in Figs. 6 and 7 were established. Under these conditions, the colliculus-only model produced slightly curved and hypometric averaging saccades, respectively. Further, the full model including the parallel signals generated highly curved saccades under the same conditions as used in Fig. 10. These results show that the model proposed here is relatively insensitive to the broadness of the tuning function used to represent SNr disinhibition.

Other external sources of modulation to the SC may provide sharper tuning that could interact with the excitatory input generated by visual inputs in addition to that of the SNr. For example, spatially tuned inputs from the FEFs, which are excitatory and topologically organized (Sommer and Wurtz 2000), could provide an advantage to a particular location on the SC map and help to dictate

target selection there. The combination of narrowly tuned excitation from FEFs, some disinhibition from the SNr near the same site, and broader surround inhibition from the remaining SNr discharge would provide very similar trajectory variability to that shown in our present simulation. Our model emphasizes the need to learn more about tuning and population discharge in structures projecting to the SC as well as about the pattern of local circuit connections in the SC before we can more fully understand the role of the SC in target selection and saccade trajectory in more natural visual surrounds.

In our effort to illustrate the possible roles played by SC/SNr in producing saccade trajectory variability we have ignored many other neural structures that undoubtedly contribute to the production of these behaviors. In particular, we have ignored the contribution made by the fixation neurons located in the rostral region of the SC and their inhibitory effect on more caudal SC neurons and facilitatory effect on omnipause neurons in the SBGs. These neurons would be extremely important in simulating the effect on saccade latency produced by search paradigms (Arai et al. 2004) and by SC lesions (Hikosaka and Wurtz 1983c). Additional feedback loops that could control saccade amplitude may also involve the central mesencephalic reticular formation (Waitzman et al. 2000).

4.3 Feedback to the SC

It has been shown in tissue-slice preparations that single-pulse electrical stimulation in the superficial layers of the SC can lead to long-lasting discharge (> 100 ms) in intermediate-layer neurons (Isa et al. 1998; Pettit et al. 1999). Most likely this prolonged discharge of intermediate layer cells is caused by the local circuit excitatory connections that exist in the SC and our model. One role of inhibitory feedback to the SC may be to reduce this extended discharge of output SC cells during saccades. Simulations with the present model suggest that feedback to the SC of eye motion signals from the SBGs is not sufficient to terminate the population discharge in SC by the end of the saccade. This suggestion is supported by physiological recordings (Anderson et al. 1998; Rodgers et al. 2003). In agreement with the suggestion of Quaia et al. (1999), we hypothesize that it is the parallel input at the level of the SGBs that counteracts this residual SC input, which would by itself produce hypermetric saccades. An alternative explanation is that it is the resumption of the inhibitory discharge from the omnipause neurons (OPNs) that snuffs out the discharge in the SBGs and ends the saccade in spite of residual input from the SC. In this scenario appropriate signals would have to generate the resumption of activity in OPNs. In addition, activity in OPNs could not explain the lowered initial eye accelerations seen in monkeys and in our simulations following elimination of the parallel path to the SBGs (Fig. 9).

Feedback of both eye-velocity and eye-displacement signals to the SC during saccades was shown in our previous model to be necessary to reproduce the pattern of activity recorded in the SC during interrupted saccades and the accuracy of these saccades (Arai et al. 1999). Anatomical and physiological evidence supports the projection of such feedback information to the SC (Hartwich-Young et al. 1990; McFarland and Fuchs 1992), but conflicting views remain about the functional role of efferent eye motion feedback to the SC (Goossens and Van Opstal 2000; Soetedjo et al. 2002).

4.4 Parallel input to brainstem burst generators

Quaia et al. (1999) have summarized the reasons why a colliculus-only model with a single feedback loop through the SC cannot produce a whole host of observed behaviors of the saccadic system. Most importantly they point out that lesions in the SC produce only transient saccadic dysmetria, while lesions of the posterior cerebellum produce dramatic and lasting dysmetria. In addition, prolonged electrical stimulation in the SC produces a site-specific maximal saccade that can end well before the electrical stimulation terminates (Stanford et al. 1996). This observation requires that some additional parallel circuitry at the level of the SBGs intervene to stop the saccade while the SC continues to output a signal driven by the stimulation.

In the Quaia et al. (1999) model, a feedback loop through the cerebellum provides the major error-correcting function in both amplitude and direction. In their model an additional feedback loop through the SC reduces its output during saccades, but only at a nominal rate not tied to saccade accuracy. The colliculus-only portion in the model of Quaia et al. (1999) does not participate in directional error correction, while in our model this portion of the system has a limited directional error-correcting role and reproduces the pattern of activity that has been recorded in the SC in monkey during saccades that curve partially toward the target. Our model also produces saccade averaging behavior that often occurs when multiple visual stimuli are present, a behavior not explored in the Quaia model.

Our model has the shortcoming that it does not implement a specific mechanism in the cerebellum that could generate the precise parallel signal needed at the SBGs to insure saccade accuracy. For straight saccades it more closely resembles the model of Dean (1995) in which the hypermetric operation of a basic control loop was assumed and then the necessary parallel signal to produce correct saccades was computed. The Dean model assumes that the basic control loop exists in the brainstem and the loop does not include the SC. It is a lumped model and therefore cannot handle multiple-target inputs and trajectory variation.

The model of Quaia et al. (1999) hypothesizes that the parallel signal from the cerebellum is generated by a moving wave of activity in that structure. The rate of travel of the wave is controlled by eye-velocity feedback from the brainstem. We do not believe that most recording studies in the cFN support this hypothesis (Fuchs et al. 1993; Thier et al. 2000), although another study provides some evidence in support of their hypothesis (Ohtsuka and Noda 1991). Until further recordings are made in the cerebellum during the types of trajectory variation that we illustrate in this report, we do not believe that informed

hypotheses can be made about the neural mechanisms in the cerebellum that could contribute to this variability.

In our model, for reasons of simplicity, we have replaced a full bilateral push-pull arrangement of the SBGs with the sign of the inputs to these generators. Thus, the input to the horizontal SBG from the parallel pathway for straight saccades is positive at movement onset. This input adds to the positive drive from the SC and produces additional eye acceleration. Similar observations have been made for the input from the cerebellum to the SBGs. Projections of each cFN are primarily excitatory to the contralateral SBG (Ohtsuka and Noda 1991). It is also well known that the contralateral cFN discharges an early burst for contralateral saccades (Ohtsuka and Noda 1991; Fuchs et al. 1993). As a contralaterally directed saccade progresses, the preponderance of activity in the cFN switches to the ipsilateral nucleus. This latter activity is thought to inhibit the activity in the active SBGs through the push-pull arrangement between SBGs in the brain stem, thus applying a deceleration to the ongoing saccade. This deceleration is simulated in our model by changing the sign of the parallel input to the SBGs. The origin of the parallel excitatory input into the vertical SBG at saccade onset is less clear (Fuchs et al. 1993; Robinson 2000) but probably also involves portions of the deep cerebellar nuclei.

We found that it was necessary to delay the onset of the signal in the parallel input to produce the trajectory shape of highly curved saccades. If the parallel signals do come from the cerebellum, as suggested by others, our prediction provides a unique marker for these signals when recordings are made in the cerebellum during curved saccade trajectories. The delay may result from a late specification of the goal of the saccade at the level of the cerebellum. The rationale for this claim is that there is clear evidence for activity correlated with early goal selection in the SC (Glimcher and Sparks 1992; Basso and Wurtz 1998; McPeek and Keller 2002b), but similar visual signals have not been recorded in the cerebellum (Ohtsuka and Noda 1991; Fuchs et al. 1993).

4.5 Conclusions

Our distributed model of the saccadic system allows the input of multiple, simulated visual stimuli and produces most of the trajectory variability seen in monkeys in multiple-target situations. It utilizes distributed input from the SNr instead of the traditionally assumed strong inhibitory lateral connections within the SC to modulate population activity in the SC during saccades. This mechanism produces activity at multiple sites in the SC that resembles activity recorded in the SC during trajectory variations. Simulations with the model show that highly curved saccades with trajectories that bend sharply toward the location of the target near the end of the movement cannot be produced by a feedback control loop that includes the SC alone. The model is altered by the addition of a parallel input along with the collicular input at the level of the burst-generating circuits in the brainstem. Computation of the signals present on the parallel inputs suggests that they may come from the cerebellum, in agreement with other recent models of the saccadic system (Dean 1995; Quaia et al. 1999). Furthermore, the model predicts that the parallel input is delayed with respect to the input from the SC during highly curved saccades.

Acknowledgement. Partially supported by NIH Grant EY-08060 to E.L. Keller.

Appendix

All simulations presented in this paper were performed using Matlab 6.5 and Simulink 5.0 on a PC with MSWindows 2000. The details of the dynamics of the brainstem model and eye plant are described here for the implementation of the full saccadic model.

The horizontal and vertical nonlinear functions of the saccadic burst generators are computed by:

$$b_h(o_h(t)) = b_R(o_h(t)) + b_L(o_h(t)) \tag{14}$$

$$b_R(o_h(t)) = \begin{cases} b_m[1-\exp(\frac{-(o_h(t)+e_0)}{b_k})], & (o_h(t) > -e_0) \\ 0, & (o_h(t) \le -e_0) \end{cases} \tag{15}$$

$$b_L(o_h(t)) = \begin{cases} -b_m[1-\exp(\frac{o_h(t)-e_0}{b_k})], & (o_h(t) < e_0) \\ 0, & (o_h(t) \ge e_0) \end{cases} \tag{16}$$

$$b_v(o_v(t)) = b_U(o_v(t)) + b_D(o_v(t)), \tag{17}$$

$$b_U(o_v(t)) = \begin{cases} b_m[1-\exp(\frac{-(o_v(t)+e_0)}{b_k})], & (o_v(t) > -e_0) \\ 0, & (o_v(t) \le -e_0) \end{cases} \tag{18}$$

$$b_D(o_v(t)) = \begin{cases} -b_m[1-\exp(\frac{o_v(t)-e_0}{b_k})], & (o_v(t) < e_0) \\ 0, & (o_v(t) \ge e_0) \end{cases} \tag{19}$$

where b_R, b_L, b_U, and b_D are the right, left, up, and downward nonlinear functions, respectively (Van Gisbergen et al. 1981). The quantities b_m, b_k, and e_0 are constants. The inputs ($o_h(t)$ and $o_v(t)$) to the SBGs are calculated by the following equations:

$$o_h(t) = \begin{cases} m_h(t), & \text{(SC – only model)} \\ m_h(t) + p_h(t), & \text{(SC and parallel model)} \end{cases} \tag{20}$$

$$o_v(t) = \begin{cases} m_v(t), & \text{(SC – only model)} \\ m_v(t) + p_v(t), & \text{(SC and parallel model)} \end{cases} \tag{21}$$

where $m_h(t)$ and $m_v(t)$ are the weighted sums of the SC outputs ((5) and (6)) and $p_h(t)$ and $p_v(t)$ are the horizontal and vertical parallel signals, respectively. Note that the signs (+ and −) of these signals to the SBGs indicate right and leftward directions for the horizontal system and up and downward directions for the vertical system, respectively.

The pulselike output from the nonlinear functions is integrated by the neural integrators to produce an eye-movement command:

$$\frac{dc_h(t)}{dt} = g \times b_h(o_h(t)), \tag{22}$$

$$\frac{dc_v(t)}{dt} = g \times b_v(o_v(t)), \tag{23}$$

where $c_h(t)$ and $c_v(t)$ are the eye-movement command signals to the horizontal and vertical eye plants, respectively, and g is a gain element.

The step signals are then combined with a scaled version (parameter k) of the pulse output from the nonlinear functions and filtered by the eye plant to produce the eye movements:

$$\tau_1\tau_2\frac{d^2E_h(t)}{dt^2}+(\tau_1+\tau_2)\frac{dE_h(t)}{dt}+E_h(t) = c_h(t)+k\times g\times b_h(o_h(t))\,, \tag{24}$$

$$\tau_1\tau_2\frac{d^2E_v(t)}{dt^2}+(\tau_1+\tau_2)\frac{dE_v(t)}{dt}+E_v(t) = c_v(t)+k\times g\times b_v(o_v(t))\,, \tag{25}$$

where $E_h(t)$ and $E_v(t)$ are, respectively, the horizontal and vertical eye positions. The feedback signals ($fb_p(t)$ and $fb_v(t)$) to the SC network are computed by:

$$\tau_3\frac{dfb_p(t)}{dt}+fb_p(t)=d_1(c_h^*(t)+c_v^*(t))\,, \tag{26}$$

$$\tau_3\frac{dfb_v(t)}{dt}+fb_v(t)=d_2(g\times b_h(o_h(t)) +g\times b_v(o_v(t)))\,, \tag{27}$$

where τ_3 is a small time constant and d_1 and d_2 are scaling parameters. Note that the horizontal and vertical eye-displacement signals, $c_h^*(t)$ and $c_v^*(t)$ in (26), come from resettable neural integrators that are separate from the absolute position integrators described by (22) and (23).

References

Anderson RW, Keller EL, Gandhi NJ, Das S (1998) Two-dimensional saccade-related population activity in superior colliculus in monkey. J Neurophysiol 80:798–817

Arai K, Das S, Keller EL, Aiyoshi E (1999) A distributed model of the saccade system: simulations of temporally perturbed saccades using position and velocity feedback. Neural Netw 12:1359–1375

Arai K, Keller EL, Edelman JA (1994) Two-dimensional neural network model of the primate saccadic system. Neural Netw 7:1115–1135

Arai K, McPeek RM, Keller EL (2004) Properties of saccadic responses in monkey when multiple competing visual stimuli are present. J Neurophysiol 91:890–900

Badler JB, Keller EL (2002) Decoding of a motor command vector from distributed activity in superior colliculus. Biol Cybern 86:179–189

Basso MA, Wurtz RH (1998) Modulation of neuronal activity in superior colliculus by changes in target probability. J Neurosci 18:7519–7534

Basso MA, Wurtz RH (2002) Neuronal activity in substantia nigra pars reticulata during target selection. J Neurosci 22:1883–1894

Bayer HM, Handel A, Glimcher PW (2004) Eye position and memory saccade related responses in substantia nigra pars reticulata. Exp Brain Res 154:428–441

Bozis A, Moschovakis AK (1998) Neural network simulations of the primate oculomotor system: III. A one-dimensional, one-directional model of the superior colliculus. Biol Cybern 79:215–231

Chou IH, Sommer MA, Schiller PH (1999) Express averaging saccades in monkeys. Vis Res 39:4200–4216

Das S, Keller EL, Arai K (1996) A distributed model of the saccadic system: the effects of internal noise. Neurocomputing 11:245–269

Dean P (1995) Modelling the role of the cerebellar fastigial nuclei in producing accurate saccades: the importance of burst timing. Neuroscience 68:1059–1077

Droulez J, Berthoz A (1991) A neural network model of sensoritopic maps with predictive short-term memory properties. Proc Natl Acad Sci USA 88:9653–9657

Edelman JA, Keller EL (1998) Dependence on target configuration of express saccade-related activity in the primate superior colliculus. J Neurophysiol 80:1407–1426

Fuchs AF, Robinson FR, Straube A (1993) Role of the caudal fastigial nucleus in saccade generation: I. Neuronal discharge patterns. J Neurophysiol 70:1723–1740

Glimcher PW, Sparks DL (1992) Movement selection in advance of action in the superior colliculus. Nature 355:542–545

Goossens HHLM, Van Opstal AJ (2000) Blink-perturbed saccades in monkey: II. Superior colliculus activity. J Neurophysiol 83:3430–3452

Grossberg S, Roberts K, Aguilar M, Bullock D (1997) A neural model of multimodal adaptive saccadic eye movement control by superior colliculus. J Neurosci 17:9706–9725

Handel A, Glimcher PW (1999) Quantitative analysis of substantia nigra pars reticulata activity during a visually guided saccade task. J Neurophysiol 82:3458–3475

Handel A, Glimcher PW (2000) Contextual modulation of substantia nigra pars reticulata neurons. J Neurophysiol 83:3042–3048

Hartwich-Young R, Nelson JS, Sparks DL (1990) The perihypoglossal projection to the superior colliculus in the rhesus monkey. Vis Neurosci 4:29–42

Hikosaka O, Wurtz RH (1983a) Visual and oculomotor functions of monkey substantia nigra pars reticulata: III. Memory-contingent visual and saccade responses. J Neurophysiol 49:1268–1284

Hikosaka O, Wurtz RH (1983b) Visual and oculomotor functions of monkey substantia nigra pars reticulata: IV. Relationship of substantia nigra to superior colliculus. J Neurophysiol 49:1285–1301

Hikosaka O, Wurtz RH (1983c) Effects on eye movements of a GABA agonist and antagonist injected into monkey superior colliculus. Brain Res 272:368–372

Isa T, Endo T, Saito Y (1998) The visuo-motor pathway in the local circuit of the rat superior colliculus. J Neurosci 18:8496–8504

Jiang H, Stein BE, McHaffie JG (2003) Opposing basal ganglia processes shape midbrain visuomotor activity bilaterally. Nature 423:982–986

Johnson RA, Wichern DW (1988) Applied multivariate statistical analysis. Prentice-Hall, Upper Saddle River, NJ, pp 273–287

Karabelas AB, Moschovakis AK (1985) Nigral inhibitory termination on efferent neurons of the superior colliculus: an intracellular horseradish peroxidase study in the cat. J Comp Neurol 239:309–329

Koch C, Ullman S (1985) Shifts in selective visual attention: towards the underlying neural circuitry. Hum Neurobiol 4:219–227

Massone LE, Khoshaba T (1995) Local dynamic interactions in the collicular motor map: a neural network model. Network 6:1–18

McFarland JL, Fuchs AF (1992) Discharge patterns in nucleus prepositus hypoglossi and adjacent medial vestibular nucleus during horizontal eye movement in behaving macaques. J Neurophysiol 68:319–336

McPeek RM, Keller EL (2002a) Superior colliculus activity related to concurrent processing of saccade goals in a visual search task. J Neurophysiol 87:1805–1815

McPeek RM, Keller EL (2002b) Saccade target selection in the superior colliculus during a visual search task. J Neurophysiol 88:2019–2034

McPeek RM, Skavenski AA, Nakayama K (2000) Concurrent processing of saccades in visual search. Vis Res 40:2499–2516

McPeek RM, Han JH, Keller EL (2003) Competition between saccade goals in the superior colliculus produces saccade curvature. J Neurophysiol 89:2577–2590

Minken AWH, Van Opstal AJ, Van Gisbergen JAM (1993) Three-dimensional analysis of strongly curved saccades elicited by double-step stimuli. Exp Brain Res 93:521–533

Munoz DP, Istvan P (1998) Lateral inhibitory interactions in the intermediate layers of the monkey superior colliculus. J Neurophysiol 79:1193–1209

Ohtsuka K, Noda H (1991) Saccadic burst neurons in the oculomotor region of the fastigial nucleus of macaque monkeys. J Neurophysiol 65:1422–1434

Optican LM (1994) Control of saccade trajectory by the superior colliculus. In: Fuchs AF, Brandt T, Büttner U, Zee DS (eds) Contemporary ocular motor and vestibular research: a tribute to David A. Robinson. Georg Thieme, Stuttgart, pp 98–105

Özen G, Helms MC, Hall WC (2004) The intracollicular neuronal network. In: Hall WC, Moschovakis AK (eds) The superior colliculus: new approaches for studying sensorimotor integration. CRC Press, Boca Raton, FL, pp 147–158

Pettit DL, Helms MC, Lee P, Augustine GJ, Hall WC (1999) Local excitatory circuits in the intermediate gray layer of the superior colliculus. J Neurophysiol 81:1424–1427

Port NL, Wurtz RH (2003) Sequential activity of simultaneously recorded neurons in the superior colliculus during curved saccades. J Neurophysiol 90:1887–1903

Quaia C, Lefèvre P, Optican LM (1999) Model of the control of saccades by superior colliculus and cerebellum. J Neurophysiol 82:999–1018

Robinson FR (2000) Role of the cerebellar posterior interpositus nucleus in saccades: I. Effect of temporary lesions. J Neurophysiol 84:1289–1302

Robinson FR, Straube A, Fuchs AF (1993) Role of the caudal fastigial nucleus in saccade generation: II. Effects of muscimol inactivation. J Neurophysiol 70:1741–1758

Rodgers KC, Munoz DP, Scott SH, Pare M (2003) The activity carried by superior colliculus neurons is not a sufficient motor command. Soc Neurosci Abstr 79(2):388

Schall JD, Thompson KG (1999) Neural selection and control of visually guided eye movements. Annu Rev Neurosci 22:241–259

Soetedjo R, Kaneko CRS, Fuchs AF (2002) Evidence that the superior colliculus participates in the feedback control of saccadic eye movements. J Neurophysiol 87:679–695

Sommer MA, Wurtz RH (2000) Composition and topographic organization of signals sent from the frontal eye field to the superior colliculus. J Neurophysiol 83:1979–2001

Stanford TR, Freedman EG, Sparks DL (1996) Site and parameters of microstimulation: evidence for independent effects on the properties of saccades evoked from the primate superior colliculus. J Neurophysiol 76:3360–3381

Takagi M, Zee DS, Tamargo RJ (1998) Effects of lesions of the oculomotor vermis on eye movements in primate: saccades. J Neurophysiol 80:1911–1931

Thier P, Dicke PW, Haas R, Barash S (2000) Encoding of movement time by populations of cerebellar Purkinje cells. Nature 405:72–76

Van Gisbergen JAM, Robinson DA, Gielen S (1981) A quantitative analysis of generation of saccadic eye movements by burst neurons. J Neurophysiol 45:417–441

Van Opstal AJ, Van Gisbergen JAM (1989) A nonlinear model for collicular spatial interactions underlying the metrical properties of electrically elicited saccades. Biol Cybern 60:171–183

Waitzman DM, Ma TP, Optican LM, Wurtz RH (1991) Superior colliculus neurons mediate the dynamic characteristics of saccades. J Neurophysiol 66:1716–1737

Waitzman DM, Silakov VL, DePalma-Bowles S, Ayers AS (2000) Effects of reversible inactivation of the primate mesencephalic reticular formation: I. Hypermetric goal-directed saccades. J Neurophysiol 83:2260–2284

Walker MF, FitzGibbon EJ, Goldberg ME (1995) Neurons in the monkey superior colliculus predict the visual result of impending saccadic eye movements. J Neurophysiol 73:1988–2003

Yuille AL, Grzywacz NM (1989) A winner-take-all mechanism based on presynaptic inhibition feedback. Neural Comput 1:334–347